coatings

MDPI

Article

Photocatalytic Behavior of Water-Based Styrene-Acrylic Coatings Containing TiO_2 Sensitized with Metal-Phthalocyanine Tetracarboxylic Acids

Valentin Raditoiu [1], Alina Raditoiu [1,*], Monica Florentina Raduly [1], Viorica Amariutei [1], Ioana Catalina Gifu [1,2] and Mihai Anastasescu [2]

[1] National Research and Development Institute for Chemistry and Petrochemistry—ICECHIM, 202 Splaiul Independentei, 060021 Bucharest, Romania; vraditoiu@icechim.ro (V.R.); radulymonica@yahoo.com (M.F.R.); vamariutei@yahoo.com (V.A.); gifu_ioanacatalina@yahoo.com (I.C.G.)

[2] Institute of Physical Chemistry "Ilie Murgulescu", 202 Splaiul Independentei, 060021 Bucharest, Romania; manastasescu@icf.ro

* Correspondence: coloranti@icechim.ro; Tel.: +40-21-688-4119

Academic Editor: Alessandro Lavacchi

Received: 6 November 2017; Accepted: 8 December 2017; Published: 12 December 2017

Abstract: The study presents the results regarding the photocatalytic behavior of some water-based styrene-acrylic coatings containing TiO_2 nanoparticles sensitized with metal-phthalocyanine tetracarboxylic acids. Coating materials have been studied in terms of color characteristics, photocatalytic behavior, and resistance to self-degradation depending on the structure of phthalocyanine sensitizers. Coatings that were exposed to Xenon light showed degradation of the organic sensitizer rather than of the binder. Photocatalytic tests using methylene blue as a standard contaminant indicated that the coating containing TiO_2 nanoparticles sensitized with Fe(III) phthalocyanine tetracarboxylic acids showed the highest efficiency both in ultraviolet or visible light. In this case, the UV light induced a photodegradation rate that was greatly increased of about fifty times comparatively with that induced by LED light and was determined by two different mechanisms, but side reactions like methylene blue and sensitizer self destruction are possible to occur simultaneously. Photocatalytic materials of this type are suitable to be used as decorative coatings especially for indoor applications.

Keywords: photocatalysts; titanium dioxide; phthalocyanines; waterborne coatings; LED light

1. Introduction

Photocatalysis represents an active field of research during the last years. Many efforts have been made in order to find new types of photocatalytic materials, which are able to promote generation of species that react with different types of organic compounds and to efficiently remove pollutants from aqueous media or from solid surfaces [1–3]. Besides classical semiconducting oxides, namely TiO_2 and ZnO, only CeO_2 has proved a convenient behavior for this type of applications, despite the rapid recombination of photo-generated electrons and holes. However, TiO_2 remains the most important photocatalyst due to its convenient semiconducting properties (band gap), outstanding chemical resistance and availability [4,5].

Photocatalytic properties of TiO_2 were intensively investigated in relationship with crystallinity, shape and size of the particles, the presence of defects, or doping compounds [6–8]. Elucidation of photocatalytic mechanisms for different types of materials, substrates, organic pollutants, and irradiation wavelengths leads to a rapid development of highly efficient photocatalytic materials based on titania. Unfortunately, photocatalytic activity of titania materials is maximum when they

are exposed to UV radiation because electron-hole pairs are efficiently generated during irradiation with light having a wavelength around 380 nm. Moreover, there are several major drawbacks of titania photocatalyst, which are due to the rapid electron-hole recombination and the wide band gap of the materials, which limits light absorption to the UV region [9,10]. In addition, UV radiation represents less than 5% of solar energy distribution and this was the main reason of the efforts made to produce photocatalysts that use visible light, which represents around 43% of solar energy [11].

As some photocatalytic materials are suitable to be used for indoor applications, many efforts are made to develop new photocatalyst, which could be used on the tunnels and the underground parking's walls that are exposed to pollution, especially due to the engines emissions. The effect could be enhanced by concomitant usage of new ecological friendly sources of artificial light, such as LED's that provide an intense level of illumination and shift the range of maximum photocatalytic efficiency in the visible light domain. Therefore, among research related to optimize nanoparticle's shape, size, and morphology [12–15] a great deal of attention was paid to the modification of titania-based photocatalyst with metal and non-metal atoms to shift the optimum range of action to the visible domain of the spectrum [16], but the recombination of photo-generated species remains an important challenge. Another strategy is related to the development of heterojunctions between semiconducting oxides and different photosensitizing materials [17–19].

Phthalocyanines can be one of the most efficient and stable class of photosensitizers for TiO_2 photocatalysts operating under visible light irradiation, as some studies have already reported [20–29], but the anchoring groups that could bind them on the nanoparticles surface [30] decisively determine the overall efficiency. Studies related to the stability of several coupling functionalities, such as carboxyl, phosphate, sulfonate, acetyl, silyl, hydroxyl, or amino reveal that carboxyl groups exhibit a very good stability during photocatalytic processes [31]. Moreover, as it had already been found, photocatalytic coatings that were based on organic binders can be obtained if an appropriate filler is used in order to reduce the photoactivity of the semiconductor and consequently to retard the self-destruction of the coating [32,33].

The objective of our work was to obtain and to evaluate visible light responsive coatings that were capable of effective photocatalysis in weak light or in the absence of UV radiation, especially for indoor applications where LEDs are used as light sources. The study should also determine the existence of a possible deactivation effect caused by the embedding of photocatalysts in the film building material by preventing the contact with the contaminant. Furthermore, it was important to elucidate if the self-degradation of the coating organic components caused by the interaction with photocatalysts occurs during the degradation processes, and which is the level of self-degradation.

2. Materials and Methods

2.1. Materials

Parmetol A26 and Parmetol DF12 were purchased from Brenntag BV Nederland (Dordrecht, The Netherlands). Dow Chemical Co. (Midland, MI, USA) provided Latex DL450, Dowanol DPnB and Cellosize HEC. OMYACARB 5TN was obtained from OMYA Int. AG (Oftringen, Switzerland), while Aeroxide P25 was provided by Evonik Ind. (Essen, Germany) BYK 034 was purchased from BYK-Chemie GmbH (Wesel, Germany) and ADDAPT DISP 500 was obtained from ADDAPT Chemicals BV (Helmond, The Netherlands). Isopropyl alcohol and aqueous ammonia solution (25 wt %) were purchased from Novachim (Bucharest, Romania), were of laboratory reagent grade and were used as received. De-ionized water was used in experiments, while we obtained metal-phthalocyanine tetracarboxylic acids (MPcTC, where M = Ni, Al, Co, Zn, Fe(III), Cu, Mn) in laboratory following a well-known method [34] and we used them as sensitizers for TiO_2.

2.2. Surface Modification of TiO_2 with Metal-Phthalocyanine Tetracarboxylic Acids

A mixture of 1.9 g TiO_2 powder (P25) and 0.05 g MPcTC was added to 50 mL isopropyl alcohol containing 0.2 mL ammonia aqueous solution (25 wt %) under vigorous stirring until a fine suspension

is obtained. The reaction mass was heated under reflux 5 h and titanium dioxide nanoparticles that were modified with MPcTC's were separated by centrifugation at 4000 rpm, washed with de-ionized water, filtered and dried in an oven, at 120 °C, for 10 h.

2.3. Characterization of TiO_2 Sensitized with Metal-Phthalocyanine Tetracarboxylic Acids

Diffuse reflectance UV-Vis spectra of powders were recorded on a Jasco V570 spectrometer (JASCO Int. Co., Ltd., Tokyo, Japan) equipped with a Jasco ILN-472 integrating sphere (150 mm), using Spectralon as a reference. The optical band gap was calculated using Jasco VWGA-589—band gap measurement software (Ver. 1.03C, JASCO Int. Co., Ltd., Tokyo, Japan). Diffuse reflectance Fourier-transform infrared (DRIFT) spectra was obtained on the photocatalytic powders mixed with KBr by using an EasiDiff accessory from Pike Techn. Inc. (Fitchburg, WI, USA) attached to a Jasco FT-IR 6300 instrument (JASCO Int. Co., Ltd., Tokyo, Japan), in the range 400–4000 cm^{-1} (30 scans at a resolution of 4 cm^{-1}). X-ray diffraction (XRD) analysis was performed on powders using a Rigaku SmartLab X-ray diffractometer (Rigaku, Tokyo, Japan) with vertical goniometer, in parallel beam geometry, at room temperature, and using a Cu Kα radiation (λ = 1.54056 Å). The morphology of the nanoparticles was examined by transmission electron microscopy (TEM) on a JEOL 200CX Scanning-Transmission (JEOL, Tokyo, Japan) Electron microscope at an accelerating voltage of 200 kV. Nitrogen sorption isotherms were recorded on a Quantachrome Nova 2200e automated gas adsorption system (Quantachrome Instruments, Boynton Beach, FL, USA), at the liquid nitrogen temperature (−196 °C). All of the samples were outgassed at 300 °C for 3 h under vacuum prior to nitrogen adsorption. BET surface area was calculated according to Brunauer-Emmett-Teller equation, total pore volume was estimated from the amount of gas adsorbed and the micropores surface area and volume were determined using t-plot analysis.

2.4. Preparation of Styrene-Acrylic Coatings

The paint formulation was provided by Chimcolor (Bucharest, Romania), and is shown in Table 1. In a typical procedure, the preservatives, defoaming agent, coalescent and dispersant were mixed with water using a double suction disc Laboratory Dissolver (ATP Engineering B.V., Almere, The Netherlands). After the pH adjustment to 9 with the aqueous ammonia solution, the binder was slowly added and the mixture was homogenized. Finally, the thickener was added to the mixture and a stirring at a rate of 1500 rpm was maintained 30 min. In order to obtain photocatalytic coatings, TiO_2 sensitized with phthalocyanines and the styrene-acrylic paint previously obtained were homogenized using an Automatic Pigment Muller (J. Engelsmann AG, Ludwigshafen am Rhein, Germany). Coatings with a thickness of 50 ± 1 μm were applied, using an Elcometer 3570 film applicator (Elcometer Ltd., Manchester, UK), on glass slides, previously degreased and cleaned in Piranha solution. The films were dried at room temperature (25 ± 2 °C) for 48 h and used as such for photocatalytic experiments and coatings characterization. Thickness of the coatings was determined with a TROTEC BB25 layer thickness-measuring device (TKL GmbH, Heinsberg, Germany).

Table 1. The formulation of waterborne coatings.

Component	Role (Active Substance)	Quantity (wt %)
Water	medium	20.3
Parmetol A26	preservative (mixture of 5-Chloro-2-methyl- and 2-Methyl-2H-isothiazol-3-one)	0.1
Parmetol DF12	preservative (mixture of isothiazolinones)	0.1
BYK 034	defoamer (mixture of paraffin based mineral oils and silicones)	0.2
ADDAPT DISP 500	dispersant (ammonium polyacrylate)	0.4
Ammonia (5 wt %) solution	pH adjustment (ammonia)	0.1
Latex DL450	binder (styrene-acrylic)	18.7
Dowanol DPnB	coalescent (dipropylene glycol *n*-butyl ether)	1
OMYACARB 5TN	filler ($CaCO_3$)	48.5
Cellosize HEC	thickener (hydroxyethyl cellulose)	10.6

2.5. Coatings Characterization and Evaluation of Photocatalytic Performances

Diffuse reflectance UV-Vis spectra were recorded on coatings that were deposited on glass slides using the same apparatus as in the case of photocatalysts. Color measurements in CIE $L^*a^*b^*$ system were performed using Jasco VWTS-581 color analysis software (Ver. 2.00A, JASCO Int. Co., Ltd., Tokyo, Japan) for a 10° standard observer and under illuminant D65. Color modifications are quantified by its attributes: hue (H^*), chroma (C^*), and lightness (L^*). The total color difference is calculated from the equation:

$$\Delta E^* = \sqrt{(\Delta L^*)^2 + (\Delta a^*)^2 + (\Delta b^*)^2} \quad (1)$$

where L^* is the lightness, a^* and b^* are red-green, respectively, yellow-blue color components and the calculated differences indicate how much the two states of a sample differ from one another, while the composition is evaluated using:

$$\Delta H^* = \sqrt{(\Delta E^*)^2 - (\Delta L^*)^2 - (\Delta C^*)^2} \quad (2)$$

where H^* is hue and C^* is chroma. A CAM 200 optical contact angle and surface tension goniometer (KSV Instruments, Helsinki, Finland) was used to assess coatings wettability. Atomic force microscopy (AFM) was performed in noncontact mode on a Park Systems XE 100 microscope (Park Systems, Suwon, Korea). Specular reflection of the coatings was measured with the Multi Gloss 268Plus gloss-meter from Konica Minolta Inc. (Tokyo, Japan).

Coating's photocatalytic activity was evaluated by performing photodegradation experiments using Methylene Blue (MB) as a model contaminant and UV-Vis spectroscopy to detect changes of MB concentration during photochemical reactions. Methylene Blue solution of 1 g/L in water was sprayed on the surface of the coatings that were deposited on glass slides, followed by drying for 2 h at 120 °C in an oven. Samples were irradiated in a homemade chamber using visible light generated by two LED projectors of 100 W each (Super Bright LEDs Inc., St. Louis, MO, USA), providing a warm white light (correlated color temperature 2700–3000 K). The irradiance of 30 ± 1 W/cm^2 was measured at the surface of the samples with a Delta OHM-HD 2302.0 Light-meter (Delta OHM Srl, Padova, Italy) equipped with LP 471 RAD radiometric probe for effective irradiance measurement in the spectral range 400–1050 nm. For comparison purposes, similar samples were irradiated in an ATLAS-Xenotest 150S+ apparatus (2200 W, Atlas Material testing Solutions, Mount Prospect, IL, USA), according to ISO 105-B02 [30] normal conditions (irradiance of 42 ± 2 W/cm^2 in the range 300–400 nm). During the photocatalytic experiments, the concentration of MB was measured from visible diffuse reflectance spectra and the degradation efficiency (%) was calculated from the most significant minimum of the reflectance spectrum using:

$$\mathrm{DE} = \frac{R_t - R_0}{R_0} \times 100 \quad (3)$$

where DE is degradation efficiency (%), R_t represents the reflectance at various intervals of exposure to light, and R_0 the initial reflectance of the coating.

Total organic carbon (TOC) was determined by using a Multi N/C 2100 TOC analyzer from Analytic Jena AG (Jena, Germany). Samples were prepared by extraction in distilled water of all the soluble species (MB, sulfonic acids and phenols are water soluble species) that were located at the surface of the initial and LED light exposed photocatalytic coatings.

3. Results and Discussion

3.1. Characterization of the Photocatalysts

In order to obtain the desired effect of increasing the photocatalytic activity in the visible range of the spectrum, it was necessary to establish the optimal concentration of sensitizer that was deposited onto the P25 surface. As a result of the experiments, a 2.5 wt % sensitizer to P25 was established as

optimal. At this concentration, maximization of visible radiation absorption is achieved, so that in the absence of UV radiation the photocatalytic processes can be carried out within acceptable time limits, at the usual loading of the studied coatings with photocatalysts, as will be further demonstrated. As a result, it ensured the avoidance of dye aggregation on P25 surface and the formation of sensitizer islands, as well as ensuring an adequate intensity of the obtained colors so that the coatings also provide a decorative effect.

The Kubelka-Munk transformed UV-Vis reflectance spectra show the presence of two Q-bands, corresponding to π–π* transitions, frequently denoted as α-Q-band and β-Q-band, situated at 607–650 nm and 668–703 nm, respectively. The first band is attributed to the formation of dimeric species, while the last one is due to monomers, as was already reported for phthalocyanine derivatives in solution [35]. In the case of all the photocatalysts, the absorption bands of phthalocyanine sensitizers are red shifted and broadened because of interactions with the solid host. It is obvious from the spectra that in the case of Fe(III)PcTC sensitized photocatalyst was obtained the largest red-shifted and broadened absorption spectrum, having a high ratio between α- and β-Q-band intensities, as can be observed in Figure 1a.

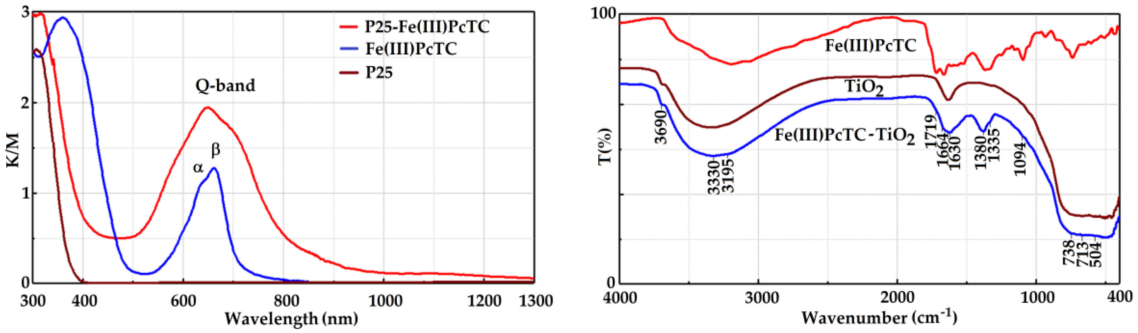

Figure 1. (**a**) Kubelka-Munk transformed reflectance spectra and (**b**) diffuse reflectance Fourier-transform infrared (DRIFT) spectra of P25-Fe(III)PcTC.

This behavior can be explained by a strong interaction between the Fe(III)PcTC monomeric species and P25 hosting material due to the presence of carboxyl strong anchoring groups in the structure of the sensitizer [31]. Furthermore, the optical band gap that was calculated from the diffuse reflectance spectra shows that photophysical properties in the visible range are significantly improved in all the cases of photocatalysts sensitized with MPcTC in comparison to P25, as can be observed in Table 2. The results demonstrate the effectiveness of the phthalocyanine sensitizers bearing carboxyl groups that will be beneficial for the photocatalytic properties in the visible range, in accordance to other reports [36].

Table 2. Absorption data and band gap of the photocatalysts.

Photocatalyst	Absorption Peaks (nm)		α/β Q-Band Intensity Ratio	Width of Q-Band Absorption Peaks (nm)	Energy Band Gap (eV)
	α-Q-Band	β-Q-Band			
P25	–	–	–	–	3.38
P25-NiPcTC	607	668	1.25	150	3.34
P25-AlPcTC	637	694	1.01	183	3.17
P25-CoPcTC	610	670	1.2	165	3.32
P25-ZnPcTC	637	686	0.97	148	3.18
P25-Fe(III)PcTC	650	703	1.17	174	3.34
P25-CuPcTC	609	678	1.25	165	2.74
P25-MnPcTC	639	674	1.01	149	3.34

The DRIFT spectra of the photocatalysts is characterized by the presence of a broad band that is centered at 3330 cm^{-1} that corresponds to the hydroxyl groups involved in hydrogen bonds and a shoulder at 3195 cm^{-1}, which is due to the stretching vibration of C–H aromatic bonds corresponding to the phthalocyanine sensitizer. Groups that are involved in such interactions can belong to carboxyl groups or hydroxyl groups on the TiO_2 surface and to adsorbed water molecules. An important peak is situated at 3690 cm^{-1} and corresponds to the stretching vibrations of hydroxyl isolated groups on the titania surface. Another important broad peak that is centered at 1630 cm^{-1} is due to the H_2O bending vibrations combined with two other bands due to the C=O stretching vibration of the carboxyl groups situated at 1719 cm^{-1}. Next to it, the –C–N= stretching vibration located at 1664 cm^{-1} as a shoulder, demonstrate the presence of the phthalocyanine sensitizer on the photocatalyst surface, as it can be observed from Figure 1b. The absorption peak at 1380 cm^{-1} may be assigned to the carboxylate ion, while at 1335 cm^{-1} is located the stretching vibration of C=C aromatic groups. Other characteristic peaks are located at 1094 and 713 cm^{-1}, due to the aromatic –CH deformation while at 738 and 504 cm^{-1} are situated bands corresponding to tetrahedron and octahedron Ti–O symmetric stretching vibrations. DRIFT spectra clearly demonstrate that the interaction between phthalocyanine sensitizers and TiO_2 is a chemical one through the carboxyl groups.

The analysis of XRD spectra, as can be seen in Figure 2a, shows that all of the diffraction peaks can be indexed to tetragonal structures of anatase and rutile, according to PDF Card Nos.: 00-064-0863 and 00-021-1276, respectively.

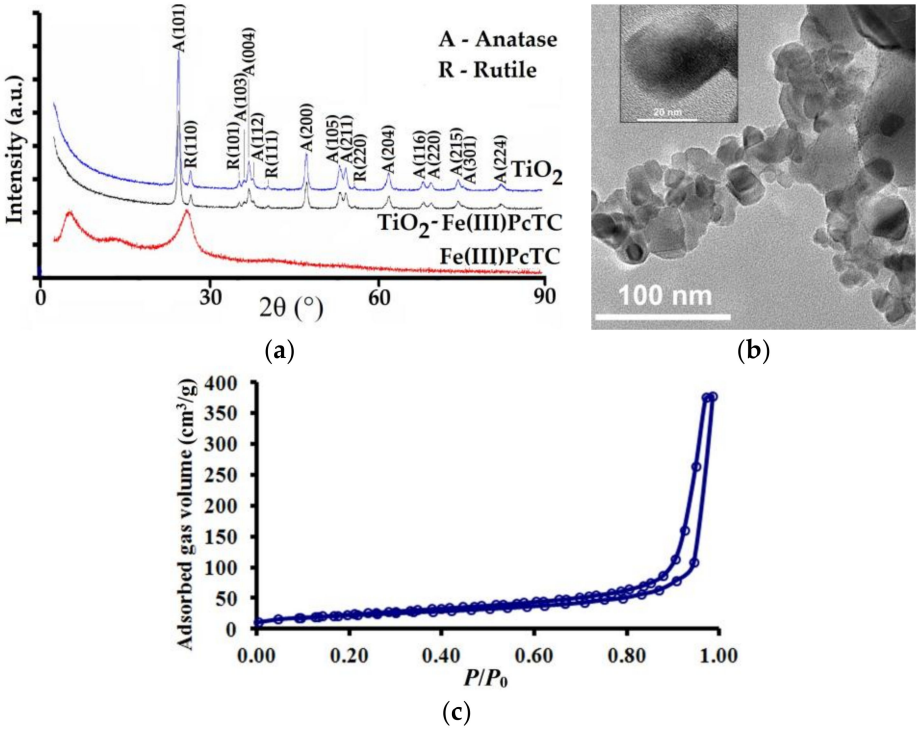

Figure 2. (**a**) X-ray diffraction (XRD) pattern; (**b**) TEM image and (**c**) nitrogen adsorption-desorption isotherm of P25-Fe(III)PcTC. P/P_0 is the ratio between the equilibrium and the saturation pressure of nitrogen.

Interplanar distances (d_{hkl}) were calculated using Bragg Equation:

$$d_{hkl} = \lambda/(2\sin\theta) \quad (4)$$

where λ is the X-ray wavelength and θ is the Bragg angle. The lattice constants of the tetragonal phases, calculated by Rietveld refinements of the diffraction data, were a = 3.7885 and c = 9.5188 Å for anatase

and a = 4.6025 and c = 2.9556 Å for rutile. The medium size of the particles was around 17–20 nm, and it was calculated from the most intense peaks of the spectrum, using Scherrer Equation:

$$D_p = 0.94\lambda/(\beta_{1/2}\cos\theta) \quad (5)$$

where D_p is the average crystallite size, $\beta_{1/2}$ is the full width at half maximum, while all of the other parameters have the same signification, as was previously stated.

The composition of P25, determined from diffraction data, is 88.8 wt % anatase and 11.2 wt % rutile remain essentially unchanged after doping with phthalocyanines. For Fe(III)PcTC, the most intense peaks were recorded at 5.51°, 14.10°, 26.84°, and 42.65° 2θ. For the other phthalocyanine sensitizers the diffraction peaks are situated in the same regions. However, if we will analyze the spectra of the photocatalysts we will observe the influence of phtalocyanine doping materials on the structure of P25 titania photocatalyst. Additionally, a shift of the peak corresponding to rutile (110) to higher 2θ angles takes place for all the photocatalysts, which is very likely caused by tensile stress, as was already observed in other cases [37]. The explanation of this behavior might be related to the existence of structure similarities between phthalocyanine sensitizers and rutile, which can lead to favorable interactions on this face of the crystals through carboxyl groups. Thereby, a characteristic peak of Fe(III)PcTC was found at 26.842°, and for rutile, (110) peak was observed at 27.375° in P25 photocatalyst, while in TiO_2-Fe(III)PcTC the peak is shifted to 27.428° 2θ. This behavior is explained by the preference of carboxyl groups to bind on the titania surface through bidentate chelating mode and the presence of four such chelating groups in the structure of phthalocyanines, together with the existence of a mixture of isomers lead to different binding geometries. However, it is clear that the structural changes that are caused by this type of interactions did not alter the crystalline structure, composition, or size of P25 photocatalyst. Evidence in this sense is represented by the similar intensity of the peaks and crystallite size of P25 nanoparticles that is not affected, as can be observed from full width at half-maximum of the peaks—about 0.51 for all of the samples.

The analysis of P25-MPcTC TEM images confirms the presence of photocatalyst nanoparticles with sizes around 20 nm and a well-defined crystalline structure that is not altered because of deposition of the sensitizer on the surface of P25 nanoparticles. Moreover, all MPcTC that are deposited onto P25 surface are not amorphous and do not exhibit filmogenic character, and there are no agglomerated particles due to the sensitizer crystallization and aggregation, as can be observed in Figure 2b.

Textural parameters define the behavior of the materials during photocatalytic processes. The nature and size of phthalocyanine sensing molecules could change essentially photocatalysts porosity or their specific surface area. However, in the case of P25 photocatalysts that were sensitized with phthalocyanines the BET (Brunauer-Emmett-Teller) surface area and the pore size do not suffer major changes, as can be observed in Table 3. Nitrogen adsoption isotherms for all the samples are similar and show a type IV hysteresis loop (Figure 2c).

Table 3. Textural properties of the photocatalysts.

Photocatalyst	BET Surface Area (m^2/g)	Pores Volume (BJH) (cm^3/g)	Micropores Diameter (BJH) (nm)
P25	57	0.43	24
P25-NiPcTC	55	0.33	24
P25-AlPcTC	56	0.34	24
P25-CoPcTC	53	0.30	24
P25-ZnPcTC	50	0.31	34
P25-Fe(III)PcTC	54	0.23	31
P25-CuPcTC	54	0.38	33
P25-MnPcTC	53	0.44	34

3.2. Coatings Properties

Water contact angle at the surface of the coatings shows a slight hydrophobic character obtained when P25 sensitized with phthalocyanine dyes is used for photocatalytic coatings. Besides the binder, only the organic dyestuff molecules, which are bound onto the surface of the P25 nanoparticles and hinder the Ti–OH groups, are able to determine the hydrophobic nature of the coatings. The hydrophobic character of the photocatalysts, and as a consequence the water contact angle of the coatings, has the highest value of about 97° in the case of P25-ZnPcTC photocatalytic coating, while the lowest value was measured for P25-NiPcTC coating, as shown in Figure 3. Surprisingly, films that are exposed to LED light show a small variation of the water contact angle after 160 h of exposure. For all of the samples, it is quite evident that a slight increase of the values was recorded during the exposure to visible light. The phenomenon is related to a possible continuation of the crosslinking process, which is common to waterborne coatings. As it is already known [38], this type of coatings is characterized by a long drying time. Therefore, only an advancement of the crosslinking process can explain the higher values of the water contact angle recorded at the end of the exposure to visible light. We can presume that this can be a reason for an increased contact area between the contaminant and the photocatalytic coatings, which will finally lead to a higher efficiency of the photodegradation process. Moreover, this important evidence allows for us to conclude that the organic binder was not affected during the photocatalytic process that was developed under visible light. Conversely, the contact angle of the coatings decrease dramatically and surfaces become hydrophilic and maintain their hydrophilic character at the end of the exposure to Xenon light generated in a Xenotest apparatus, as can be observed from Figure 3.

This is another important finding, which can signify a higher self-cleaning property of the coatings and the impossibility of pollutant molecules to adhere to the hydrophilic substrate. In this way, pollutants can be removed by washing from the coating's surface.

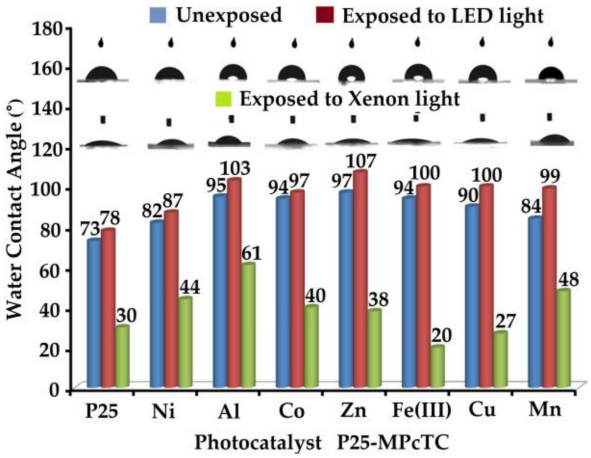

Figure 3. Water contact angle of photocatalytic coatings before and after exposure to LED and Xenon light.

However, the hydrophilic character can be evidence of the binder photodegradation, and this was the reason to investigate the changes that was suffered by the coatings during the exposure to Xenon light, using AFM measurements. As it is observed from Figure 4 in the case of LED light treated coatings, there is an increase in average roughness parameter (R_a) and root mean square roughness (R_q) from the initial values of 49.021 and 62.286 nm to 65.436 and 82.928 nm, respectively. On the contrary, in the case of Xenon light treated samples, the same parameters decrease to 35.481 and 46.570 nm.

Surprisingly, there is a slight roughing of the coating surface during LED light irradiation, which is probably due to aggregation of the photocatalyst nanoparticles in the organic binder based on their incompatibility with the polymeric matrix that is further crosslinked. This phenomenon probably

takes place by the displacement of the photocatalyst from the matrix around the larger filler particles. This displacement is sustained by the larger differences of 140 nm between the maximum valley depth (Min.) of the LED light exposed coating (Figure 4b) and of the unexposed coating (Figure 4a), comparatively with the difference of only 50 nm between the maximum peak height (Max.) of the same coatings.

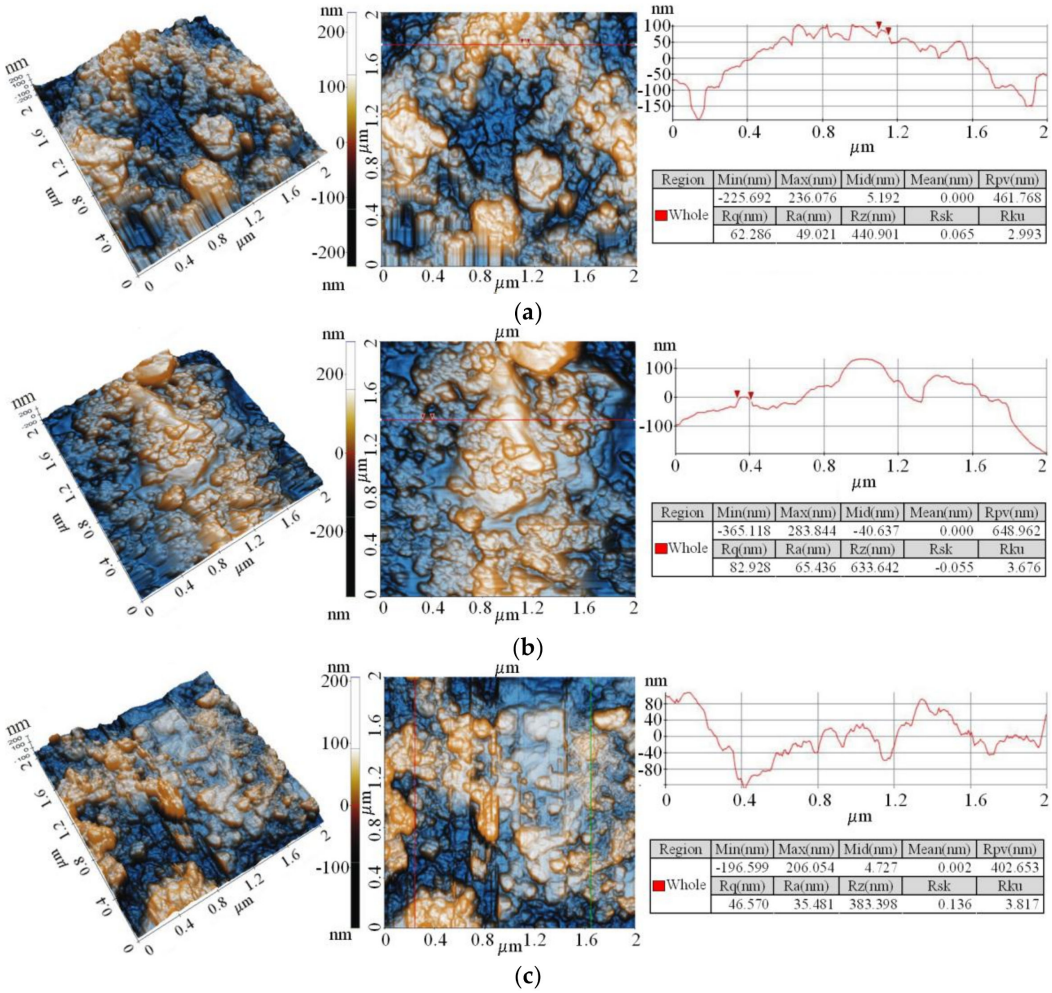

Figure 4. Atomic force microscopy (AFM) images of the photocatalytic coating containing 10 wt % P25-Fe(III)PcTC (**a**) before and (**b**) after exposure to LED light for 156 h; and (**c**) to Xenon light for 72 h.

Apparently, after UV irradiation there is a smoothing of the initial surface, which is probably due to the coating leveling. This is sustained by the values of the root mean square roughness of the sample exposed to Xenon light comparatively with that unexposed. Particularly, it should be noted that in this case the difference between the maximum valley depth (Min.) of the Xenon light exposed surface (Figure 4c) and of the initial surface (Figure 4a), has the same magnitude as the difference between the maximum peak high of the same samples. This finding sustains the leveling phenomenon and excludes the possible degradation of the binder under UV radiation.

Gloss measurement is frequently used to identify coatings photodegradation [39], which is usually accompanied by a reduction of the gloss values. Therefore, after the study of surface roughness coatings were analyzed by measuring gloss before and after exposure to LED light and to a Xenon lamp. The results confirm that the samples can be classified as low-gloss coatings due to a higher content in inorganic components, which determine a diffuse reflection of light, diminishing scattered light, and consequently, the samples gloss. Thus, measurements at 85° indicate small differences between samples before and after LED illumination or after exposure to Xenon lamp, as can be observed from

Table 4. The results sustain us to conclude that there is no evidence regarding important degradation of the binder during exposure to different type of light and coatings present good retention of the initial gloss.

Table 4. Gloss of the photocatalytic coatings.

Photocatalyst	Gloss (Gloss Units)		
	Initial	LED Light	Xenon Light
–	21.2	19.4	9.8
P25	16.8	14.5	11.9
P25-NiPcTC	22.6	16.9	14.7
P25-AlPcTC	23.7	17.8	13.8
P25-CoPcTC	22.6	17.8	19.1
P25-ZnPcTC	19.6	16.6	18.7
P25-Fe(III)PcTC	17.3	10.8	14.3
P25-CuPcTC	20.2	18.7	18.5
P25-MnPcTC	18.1	16.8	11.6

As it was already shown [40], the binder photodegradation is more pronounced as the photocatalyst loadings in the coating materials becomes higher. Therefore, in order to analyze the possible surface degradation color measurements were performed on coatings containing 10% *w*/*w* photocatalyst. According to the results obtained in the case of LED light illumination, we can observe only small variations of the color parameters for all photocatalytic coatings, as can be observed from Figure 5. This is probably due to dehydration and crosslinking process which can lead to a different environment around the photocatalyst, indicating that the binder was not visibly affected during exposure to LED light.

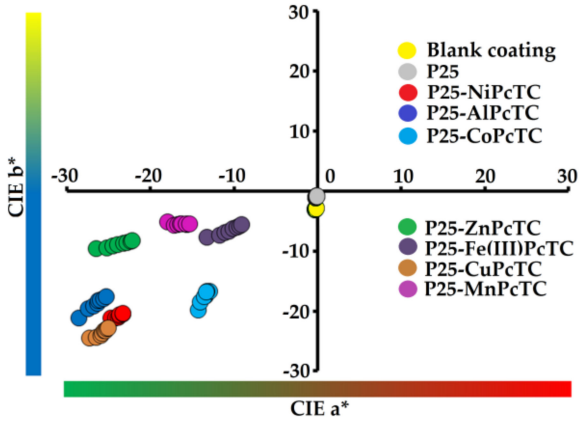

Figure 5. The evolution of CIE *a** and *b** color parameters of the photocatalytic coatings during exposure to LED light.

However, when the samples were exposed up to 72 h to Xenon light, the total color differences against the initial samples are notable and are due almost exclusively to changes of chroma (*C*), as can be seen in Table 5. Therefore, it is essential to note that this type of coatings is more suitable for indoor applications, in the absence of a suitable UV absorber or HALS in the coating material. In depth data analysis reveals a higher stability of the binder at UV radiation comparatively with the dyes used as titania sensitizers. In all of the cases studied by us, after exposure to Xenon light, the photocatalytic coatings become lighter ($\Delta L > 0$) and duller ($\Delta C < 0$). This behavior is mainly due to the dyes photodegradation, while in the case of the coating containing only P25, during exposure to Xenon light, the shade becomes yellowish ($\Delta b > 0$) and total color difference is perceptible through

close observation by human eyes. Conversely, the shade of the coatings containing P25 sensitized with MPcTC becomes reddish during exposure to Xenon light and total color differences are ten times higher than in the previous case. The major influence on the magnitude of ΔE is determined by the chroma difference (ΔC), which represents about 70%–80%, and sustains the hypothesis of sensitizer photodegradation rather than binder photodecomposition.

Table 5. Color changes of the photocatalytic coatings after 72 h of exposure to Xenon light.

Photocatalyst	Total Color Changes					
	ΔE^*	Δa^*	Δb^*	ΔL^*	ΔC^*	ΔH^*
–	1.65	−0.11	0.53	−1.56	−0.51	0.2
P25	2.57	−0.06	2.02	1.58	−1.86	0.81
P25-NiPcTC	21.38	15.31	10.34	10.76	−18.41	1.58
P25-AlPcTC	23.24	18.31	10.51	9.72	−20.92	2.87
P25-CoPcTC	16.60	8.61	10.64	9.39	−13.68	0.47
P25-ZnPcTC	18.80	17.07	3.81	6.89	−16.52	5.75
P25-Fe(III)PcTC	15.02	9.86	2.34	11.08	−9.16	4.34
P25-CuPcTC	21.98	14.11	11.92	11.91	−18.45	1.01
P25-MnPcTC	12.15	10.61	2.01	5.58	−10.63	1.88

3.3. Coatings Photocatalytic Performances

The photocatalytic styrene-acrylic coatings were comparatively tested for the degradation of MB under UV and visible light irradiation. Since the waterborne varnishes formulation is the same and photocatalytic materials are obtained in the same manner using P25 as a semiconducting oxide, while coatings with the same thickness are obtained similarly, it is quite evident that photocatalytic properties of the coating materials are only influenced by the type of sensitizing dye and photocatalyst loading.

Experimental data suggest that in UV light, the photocatalytic activity is essentially increased due to the processes that are generated at the surface of P25. The results are in accordance with two types of different mechanisms governing the photocatalytic process during LED light illumination and under UV-Vis light that is generated by a Xenon lamp. In the first case, the sensitizer is excited and electrons are injected in the conduction band (CB) of the photocatalyst producing the oxidized form of the dye, while the valence band (VB) remains unaffected. The regeneration is realized by accepting an electron from an organic specium, which is subsequently decomposed. Under UV light electrons photogenerated in the CB react with oxygen to form superoxide radicals or hydroperoxides, while holes in the VB react with adsorbed water and generate hydroxyl radicals, which oxidizes pollutants, as already demonstrated in other works [41].

Results show that under Xenon light irradiation, excepting two types (P25-NiPcTC and P25-AlPcTC) of photocatalytic coatings, all of the others studied by us completely and shortly degraded MB, as it can be observed in Figure 6a. Differences between them are related to the duration of the photocatalytic process in order to complete photodegradation of MB deposited onto the surface of the photocatalytic coatings.

However, coating containing P25-Fe(III)PcTC decomposes MB faster than the others, about four times faster than the coating containing P25 and about three times faster than P25-CuPcTC coating, which is the next in order of efficiency. It should be noted that in the same conditions of illumination, after 300 min only 65% of the MB present onto the surface of the coatings containing P25-NiPcTC and P25-AlPcTC, respectively, was decomposed.

The results obtained after LED light irradiation reveal that the most efficient photocatalytic coating is P25-Fe(III)PcTC, also, but the photocatalytic process is slower than in the previous case. Therefore, in this case, the photodegradation of MB is completely achieved after 50 h of exposure; while, after 160 h of exposure, coating containing P25 decomposes only 40% of MB, as it can be seen in Figure 6b. Surprisingly, in the case of the coating containing P25 the photodegradation of MB occurs with low

efficiency even in the absence of ultraviolet light. This behavior can be explained mainly by the sensitization effect of MB itself at the TiO_2 surface, as already reported by other authors [42].

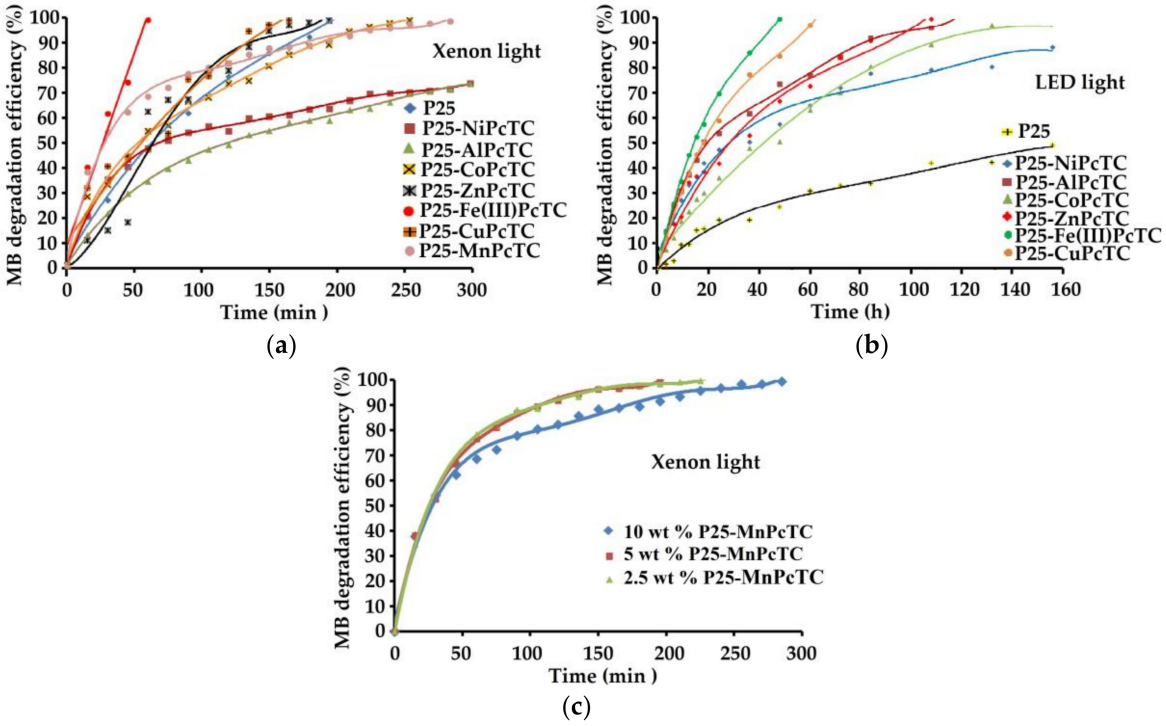

Figure 6. Methylene Blue (MB) degradation efficiency: (**a**) under Xenon light exposure; (**b**) under LED light exposure at a photocatalyst loading of 10 wt %; and (**c**) under Xenon light exposure as a function of photocatalyst loading.

When comparing the order of efficiency of the photocatalytic coatings with phthalocyanine sensitizers, it is found that it varies in the following order: Fe(III) > Cu > Zn > Co > Ni, regardless of the illuminant. It is obvious that the metal ion of the sensitizer determines the energetic levels of the photocatalyst and therefore the overall efficiency of the photocatalytic processes. This is another factor, which influences photocatalytic efficiency together with the two previously mentioned mechanisms that are determined by the exciting light.

Finally, the influence of catalyst concentration in photocatalytic coating on the efficiency of MB degradation was analyzed. As was reported by other authors [43], MB decomposition rate usually increases with the photocatalyst concentration up to a limit. In the case of the coatings containing P25-MnPcTC, as it can be observed from Figure 6c, the rate of MB photodecomposition is influenced by the catalyst concentration. The maximum rate was recorded when the photocatalyst loading is about 5 wt % in the coating material. At this concentration of photocatalyst, the time necessary for MB total photodecomposition during exposure to Xenon light is reduced with about 35% than in the case of the coating containing 10 wt % photocatalyst. Further diminishing the photocatalysts loading at 2.5 wt % reduces the rate of MB degradation. The experimental data showed similar results in the case of the other photocatalytic coatings and sustain other results already reported [44].

In order to evaluate whether MB is completely mineralized TOC loss was determined for each sample of photocatalytic coating after exposure to LED light. The initial TOC value recorded in the case of the most performing coating (Fe(III)PcTC) containing MB deposited onto the surface was 56.4 mg/L, while at the end of the exposure to LED light, determined when MB was totally discolored, the TOC value become 10.4 mg/L. The later value represents a TOC loss of about 80%, while for the other samples, the degree of TOC loss is almost the same there are three exceptions, CoPcTC and NiPcTC with about 60% and 50%, respectively, and only 20% in the case of P25 coating.

Surprisingly, mineralization takes place, to a certain degree, even in the case of P25, under visible light, due to the sensitizing effect of MB adsorbed onto the P25 surface.

The results showed that total mineralization of MB does not accompany the photobleaching during exposure to visible light even in the case of the most performing photocatalytic coating, as was already observed by other authors [45]. An explanation could be the generation of organic and inorganic acids during mineralization, which consequently determine a decrease of the pH value at the photocatalyst surface. Phenols obtained during mineralization are hard to be further oxidized in such conditions.

Concerning about the photobleaching of MB, that can be due to a reduction process to leuco methylene blue (LMB) was eliminated by the decreased TOC values obtained after irradiation, for all of the samples. However, as already demonstrated [46,47], the reduction process is possible only if oxygen is absent and a sacrificial electron donor is present. Otherwise, in aerobic conditions, small quantities of LMB eventually formed are oxidized and the original color of MB is rapidly restored [41].

The mechanism for the visible light driven generation of reactive species able to determine photocatalytic decomposition of MB onto P25 sensitized with MPcTC's is shown in Figure 7.

The process is initiated by the excitation of MPcTC ground state to its singlet excited state, which can be further transformed into the triplet state by intersystem crossing following the Path (1). The last specium can transfer energy to molecular oxygen to generate singlet oxygen following the Path (3) or superoxide anion radical by Process (4). In another Process (2), electrons from the lowest unoccupied molecular orbital (LUMO) of the MPcTC singlet excited state are injected into the conduction band (CB) of P25 and react with molecular oxygen to generate superoxide anion radical by Process (6). Finally, the radical cation of MPcTC, formed during excitation, react with water that is present at the surface of the photocatalyst and generate strongly oxidizing hydroxyl radicals, following the Path (5).

Photocatalytic degradation pathway of MB was described by other authors [48] who identify the intermediates generated during mineralization by GC-MS and LC-MS. Different aromatic amines, sulphonic acids, and phenols were detected in the photocatalytic degradation process of MB. The initiation can be ascribed to an attack of hydroxyl radical to the sulfur atom of the phenothiazine ring, followed by the formation of a sulfoxide [48]. This process induces the opening of the central aromatic ring, while the sulfoxide is further oxidized to sulfone causing the dissociation of the benzene rings and formation of sulfonic acids, which are transformed into phenols.

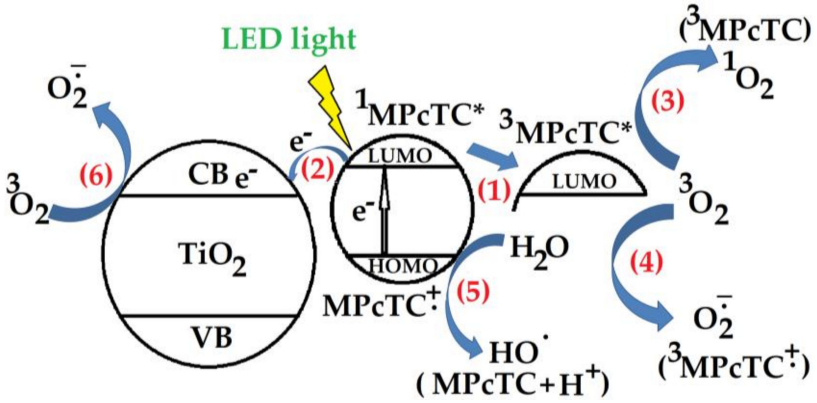

Figure 7. Mechanism for the visible light-driven generation of reactive species at the surface of the photocatalysts.

4. Conclusions

The study revealed the effect of some metal-phthalocyanine tetracarboxylic acids sensitizers on the photocatalytic efficiency of TiO_2 nanoparticles that are embedded in water-based styrene-acrylic coatings. Color characteristics, photocatalytic behavior and resistance of the coating materials to

self-degradation were investigated in relationship with the structure of phthalocyanine sensitizers. Despite the deficiencies caused by the loading of the coating materials with inorganic compounds at the expense of organic resin, the color, gloss, and roughness measurements concluded that when exposed to Xenon light, the degradation of the organic sensitizer rather than of the binder occurred, while there are no noticeable changes after the exposure to LED light. Comparative tests were developed using methylene blue as a standard contaminant and absorbance was monitored at various intervals of time during irradiation with Xenon or LED light, in order to examine the photocatalytic performance of the coatings. The results indicated that the photocatalytic coating containing TiO_2 nanoparticles sensitized with Fe(III) phthalocyanine tetracarboxylic acids showed the highest efficiency both in ultraviolet or visible light. The difference between the results of the two types of exposure was determined by the distinct mechanisms of the photocatalytic processes and was reflected in the variable duration of the processes. Dyes degradation during UV exposure and lighter colors of the photocatalytic coatings recommend them as valuable candidates for decorative coatings, which can be used for indoor applications, in the absence of suitable UV stabilizers.

Supplementary Materials: The following are available online at http://www.mdpi.com/2079-6412/7/12/229/s1, Figure S1: The emission spectrum of the LED projectors (characteristics can be found on the producer's website: superbrightleds.com).

Acknowledgments: This work was performed through Partnerships in priority areas Program—PNII-PCCA-2013-4—developed with the support of MEN-UEFISCDI, project number 0864 and Nucleu Program, project 16.31.03.03.

Author Contributions: Valentin Raditoiu obtained and characterized titania photocatalysts sensitized with dyes; Alina Raditoiu performed measurements by optical spectroscopy, analyzed and discussed the results; Monica Florentina Raduly obtained phthalocyanine sensitizers and performed BET measurements; Viorica Amariutei obtained photocatalytic coatings and performed photodegradation experiments; Ioana Catalina Gifu analyzed variations of the coatings hydrophobic character by water contact angle measurements; Mihai Anastasescu analyzed coatings surface topography by AFM measurements; Valentin Raditoiu analyzed all the experimental data and wrote the paper.

Conflicts of Interest: The authors declare no conflict of interest.

References

1. Mills, A.; O'Rourke, C.; Moore, K. Powder semiconductor photocatalysis in aqueous solution: An overview of kinetics-based reaction mechanisms. *J. Photochem. Photobiol. A* **2015**, *310*, 66–105. [CrossRef]
2. Bayrak, R.; Albay, C.; Koc, M.; Altin, I.; Degirmencioglu, I.; Sokmen, M. Preparation of phthalocyanine/TiO_2 nanocomposites for photocatalytic removal of toxic Cr(VI) ions. *Proc. Saf. Environ. Prot.* **2016**, *102*, 294–302. [CrossRef]
3. Salinas-Guzman, R.R.; Guzman-Mar, J.L.; Hinojosa-Reyes, L.; Peralta-Hernandez, J.M.; Hernandez-Ramirez, A. Enhancement of cyanide photocatalytic degradation using sol-gel ZnO sensitized with cobalt phthalocyanine. *J. Sol-Gel Sci. Technol.* **2010**, *54*, 1–7. [CrossRef]
4. Cozzoli, P.D.; Kornowski, A.; Weller, H. Low-temperature synthesis of soluble and processable organic-capped Anatase TiO_2 nanorods. *J. Am. Chem. Soc.* **2003**, *125*, 14539–14548. [CrossRef] [PubMed]
5. Xagas, A.P.; Androulaki, E.; Hiskia, A.; Falaras, P. Preparation, fractal surface morphology and photocatalytic properties of TiO_2 films. *Thin Solid Films* **1999**, *357*, 173–178. [CrossRef]
6. Tomovska, R.; Daniloska, V.; Asua, J.M. Surface modification of TiO_2 nanoparticles via photocataliticaly induced reaction: Influence of functionality of silane coupling agent. *Appl. Surf. Sci.* **2013**, *264*, 670–673. [CrossRef]
7. Rahimi, R.; Moghaddas, M.M.; Zargari, S. Investigation of the anchoring silane coupling reagent effect in porphyrin sensitized mesoporous V–TiO_2 on the photodegradation efficiency of methyl orange under visible light irradiation. *J. Sol-Gel Sci. Technol.* **2013**, *65*, 420–429. [CrossRef]
8. Stefanov, B.I.; Kaneva, N.V.; Li Puma, G.; Dushkin, C.D. Novel integrated reactor for evaluation of activity of supported photocatalytic thin films: Case of methylene blue degradation on TiO_2 and nickel modified TiO_2 under UV and visible light. *Colloids Surf. A* **2011**, *382*, 219–225. [CrossRef]

9. Madhu Kumar, P.; Badrinarayanan, S.; Sastry, M. Nanocrystalline TiO_2 studied by optical, FTIR and X-ray photoelectron spectroscopy: Correlation to presence of surface states. *Thin Solid Films* **2000**, *358*, 122–130. [CrossRef]
10. Akpan, U.G.; Hameed, B.H. Parameters affecting the photocatalytic degradation of dyes using TiO_2-based photocatalysts: A review. *J. Hazard. Mater.* **2009**, *170*, 520–529. [CrossRef] [PubMed]
11. Kruse, O.; Rupprecht, J.; Mussgnug, J.H.; Dismukes, G.C.; Hankamer, B. Photosynthesis: A blueprint for solar energy capture and biohydrogen production technologies. *Photochem. Photobiol. Sci.* **2005**, *4*, 957–970. [CrossRef] [PubMed]
12. Suttponparnit, K.; Jiang, J.; Sahu, M.; Suvachittanont, S.; Charinpanitkul, T.; Biswas, P. Role of surface area, primary particle size and crystal phase on titanium dioxide nanoparticle dispersion properties. *Nanoscale Res. Lett.* **2010**, *6*, 27. [CrossRef] [PubMed]
13. Liu, G.; Wang, X.; Chen, Z.; Cheng, H.; Lu, G. The role of crystal phase in determining photocatalytic activity of nitrogen doped TiO_2. *J. Colloid Interface Sci.* **2009**, *329*, 331–338. [CrossRef] [PubMed]
14. Chang, J.A.; Vithal, M.; Back, I.C.; Seok, S.I. Morphological and phase evolution of TiO_2 nanocrystals prepared from peroxotitanate complex aqueous solution: Influence of acetic acid. *J. Solid State Chem.* **2009**, *182*, 749–756. [CrossRef]
15. Lee, J.W.; Othman, M.R.; Eom, Y.; Lee, T.G.; Kim, W.S.; Kim, J. The effects of sonification and TiO_2 deposition on the micro-characteristics of the thermally treated SiO_2/TiO_2 spherical core-shell particles for photo-catalysis of methyl orange. *Microporous Mesoporous Mater.* **2008**, *116*, 561–568. [CrossRef]
16. Rehman, S.; Ullah, R.; Butt, A.M.; Gohar, N.D. Strategies of making TiO_2 and ZnO visible light active. *J. Hazard. Mater.* **2009**, *170*, 560–569. [CrossRef] [PubMed]
17. Chowdhury, M.; Ntiribinyange, M.; Nyamayaro, K.; Fester, V. Photocatalytic activities of ultra-small β-FeOOH and TiO_2 heterojunction structure under simulated solar irradiation. *Mater. Res. Bull.* **2015**, *68*, 133–141. [CrossRef]
18. Rawal, S.B.; Chakraborty, A.K.; Lee, W.I. Heterojunction of FeOOH and TiO_2 for the formation of visible light photocatalyst. *Bull. Korean Chem. Soc.* **2009**, *30*, 2613–2616.
19. Banerjee, S.; Pillai, S.C.; Falaras, P.; O'Shea, K.E.; Byrne, J.A.; Dionysiou, D.D. New insights into the mechanism of visible light photocatalysis. *J. Phys. Chem. Lett.* **2014**, *5*, 2543–2554. [CrossRef] [PubMed]
20. Vallejo, W.; Diaz-Uribe, C.; Cantillo, A. Methylene blue photocatalytic degradation under visible irradiation on TiO_2 thin films sensitized with Cu and Zn tetracarboxy-phthalocyanines. *J. Photochem. Photobiol. A* **2015**, *299*, 80–86. [CrossRef]
21. Zhao, X.; Li, Z.; Chen, Y.; Shi, L.; Zhu, Y. Enhancement of photocatalytic degradation of polyethylene plastic with CuPc modified TiO_2 photocatalyst under solar light irradiation. *Appl. Surf. Sci.* **2008**, *254*, 1825–1829. [CrossRef]
22. Wang, S.; Fang, Y.; Yang, Y.; Liu, J.; Deng, A.; Zhao, X.; Huang, Y. Catalysis of organic pollutant photodegradation by metal phthalocyanines immobilized on TiO_2@SiO_2. *Chin. Sci. Bull.* **2011**, *56*, 969–976. [CrossRef]
23. Machado, A.E.H.; Franca, M.D.; Velani, V.; Magnino, G.A.; Velani, H.M.M.; Freitas, F.S.; Muller, P.S., Jr.; Sattler, C.; Scmucker, M. Characterization and evaluation of the efficiency of TiO_2/Zinc phthalocyanine nanocomposites as photocatalysts for wastewater treatment using solar irradiation. *Int. J. Photoenergy* **2008**, *2008*, 482373. [CrossRef]
24. Ino, D.; Watanabe, K.; Takagi, N.; Matsumoto, Y. Electron transfer dynamics from organic adsorbate to a semiconductor surface: Zinc phthalocyanine on TiO_2(110). *J. Phys. Chem. B* **2005**, *109*, 18018–18024. [CrossRef] [PubMed]
25. Palmisano, G.; Gutierrez, M.C.; Ferrer, M.L.; Gil-Luna, M.D.; Augugliaro, V.; Yurdakal, S.; Pagliaro, M. TiO_2/ORMOSIL thin films doped with phthalocyanine dyes: New photocatalytic devices activated by solar light. *J. Phys. Chem. C* **2008**, *112*, 2667–2670. [CrossRef]
26. He, J.; Hagfeldt, A.; Lindquist, S.E.; Grennberg, H.; Korodi, F.; Sun, L.; Akermark, B. Phthalocyanine-sensitized nanostructured TiO_2 electrodes prepared by a novel anchoring method. *Langmuir* **2001**, *17*, 2743–2747. [CrossRef]
27. Rodriguez, H.B.; Di Iorio, Y.; Meichtry, J.M.; Grela, M.A.; Litter, M.; Roman, E.S. Evidence on dye clustering in the sensitization of TiO_2 by aluminum phthalocyanine. *Photochem. Photobiol. Sci.* **2013**, *12*, 1984–1990. [CrossRef] [PubMed]

28. Kim, H.J.; Jeon, J.D.; Chung, J.W.; Kwak, S.Y. Amplified visible light photocatalytic activity of mesoporous TiO_2/ZnPc hybrid by cascade Mie light scattering. *Microporous Mesoporous Mater.* **2016**, *227*, 169–175. [CrossRef]
29. Beyrhouty, M.; Sorokin, A.B.; Daniele, S.; Hubert-Pfalzagraf, L.G. Combination of two catalytic sites in a novel nanocrystalline TiO_2–iron tetrasulfophthaocyanine material provides better catalytic properties. *New J. Chem.* **2005**, *29*, 1245–1248. [CrossRef]
30. Pei, D.; Luan, J. Development of visible light-responsive sensitized photocatalysts. *Int. J. Photoenergy* **2012**, *2012*, 262831. [CrossRef]
31. Raza, M.; Bachinger, A.; Zahn, N.; Kickelbick, G. Interaction and UV-stability of various organic capping agents on the surface of anatase nanoparticles. *Materials* **2014**, *7*, 2890–2912. [CrossRef] [PubMed]
32. Pazokifard, S.; Esfandeh, M.; Mirabedini, S.M. Photocatalytic activity of water-based acrylic coatings containing fluorosilane treated TiO_2 nanoparticles. *Prog. Org. Coat.* **2014**, *77*, 1325–1335. [CrossRef]
33. Mirabedini, A.; Mirabedini, S.M.; Babalon, A.A.; Pazokifard, S. Synthesis, characterization and enhanced photocatalytic activity of TiO_2/SiO_2 nanocomposite in an aqueous solution and acrylic-based coatings. *Prog. Org. Coat.* **2011**, *72*, 453–460. [CrossRef]
34. Sun, X.; Wang, L.; Tan, Z. Improved synthesis of soluble metal-free/metal phthalocyanine tetracarboxylic acids and their application in the catalytic epoxidation of cyclohexene. *Catal. Lett.* **2015**, *145*, 1094–1102. [CrossRef]
35. Sorokin, A.B.; Buisson, P.; Pierre, A.C. Encapsulation of iron phthalocyanine in sol-gel materials. *Microporous Mesoporous Mater.* **2001**, *46*, 87–98. [CrossRef]
36. Zhou, X.; Ji, H.; Huang, X. Photocatalytic degradation of Methyl Orange over metalloporphyrins supported on TiO_2 Degussa P25. *Molecules* **2012**, *17*, 1149–1158. [CrossRef] [PubMed]
37. Grinter, D.C.; Nickels, P.; Woolcot, T.; Basahel, S.N.; Obaid, A.Y.; Al-Ghamdi, A.A.; El-Mossalamy, S.H.; Alyoubi, A.O.; Thornton, G. Binding of a benzoate dye-molecule analogue to rutile titanium dioxide surfaces. *J. Phys. Chem. C* **2012**, *116*, 1020–1026. [CrossRef]
38. Allen, N.S.; Edge, M.; Ortega, A.; Liauw, C.M.; Stratton, J.; McIntyre, R.B. Behaviour of nanoparticle (ultrafine) titanium dioxide pigments and stabilizers on the photooxidative stability of water based acrylic and isocyanate based acrylic coatings. *Polym. Degrad. Stab.* **2002**, *78*, 467–478. [CrossRef]
39. Allen, N.S.; Edge, M.; Verran, J.; Stratton, J.; Maltby, J.; Bygott, C. Photocatalytic titania based surfaces: Environmental benefits. *Polym. Degrad. Stab.* **2008**, *93*, 1632–1646. [CrossRef]
40. Allen, N.S.; Edge, M.; Ortega, A.; Sandoval, G.; Liauw, C.M.; Verran, J.; Stratton, J.; McIntyre, R.B. Degradation and stabilization of polymers and coatings: Nano versus pigmentary titania particles. *Polym. Degrad. Stab.* **2004**, *85*, 927–946. [CrossRef]
41. Chatterjee, D. Effect of excited state redox properties of dye sensitizers on hydrogen production through photo-splitting of water over TiO_2 photocatalyst. *Catal. Commun.* **2010**, *11*, 336–339. [CrossRef]
42. Barbero, N.; Vione, D. Why dyes should not be used to test the photocatalytic activity of semiconductor oxides. *Environ. Sci. Technol.* **2016**, *50*, 2130–2131. [CrossRef] [PubMed]
43. Wu, C.H.; Chern, J.M. Kinetics of photocatalytic decomposition of methylene blue. *Ind. Eng. Chem. Res.* **2006**, *45*, 6450–6457. [CrossRef]
44. Allen, N.S.; Edge, M.; Sandoval, G.; Verran, J.; Stratton, J.; Maltby, J. Photocatalytic coatings for environmental applications. *Photochem. Photobiol.* **2005**, *81*, 279–290. [CrossRef] [PubMed]
45. Mills, A.; Hill, C.; Robertson, P.K.J. Overview of the current ISO tests for photocatalytic materials. *J. Photochem. Photobiol. A* **2012**, *237*, 7–23. [CrossRef]
46. Mills, A. An overview of the methyl blue ISO test for assessing the activities of photocatalytic films. *Appl. Catal. B* **2012**, *128*, 144–149. [CrossRef]
47. Mills, A.; McFarlane, M. Current and possible future methods of assessing the activities of photocatalyst films. *Catal. Today* **2007**, *129*, 22–28. [CrossRef]
48. Houas, A.; Lachheb, H.; Ksibi, M.; Elaloni, E.; Guillard, C.; Herrmann, J.M. Photocatalytic degradation pathway of methylene blue in water. *Appl. Catal. B* **2001**, *31*, 145–157. [CrossRef]